

Journal of Materials Chemistry A

Accepted Manuscript



This is an *Accepted Manuscript*, which has been through the Royal Society of Chemistry peer review process and has been accepted for publication.

Accepted Manuscripts are published online shortly after acceptance, before technical editing, formatting and proof reading. Using this free service, authors can make their results available to the community, in citable form, before we publish the edited article. We will replace this *Accepted Manuscript* with the edited and formatted *Advance Article* as soon as it is available.

You can find more information about *Accepted Manuscripts* in the [Information for Authors](#).

Please note that technical editing may introduce minor changes to the text and/or graphics, which may alter content. The journal's standard [Terms & Conditions](#) and the [Ethical guidelines](#) still apply. In no event shall the Royal Society of Chemistry be held responsible for any errors or omissions in this *Accepted Manuscript* or any consequences arising from the use of any information it contains.



Journal Name

ARTICLE

A low-temperature benzyl alcohol/benzyl mercaptan synthesis of iron oxysulfide/iron oxide composite materials for electrodes in Li-ion batteries

Received 00th January 20xx,
Accepted 00th January 20xx

DOI: 10.1039/x0xx00000x

www.rsc.org/

S. Sallard,^a E. Castel,^a C. Villevieille^a and Petr Novák^a

A low-temperature reaction of benzyl alcohol/benzyl mercaptan with iron (III) acetylacetonate was used to synthesize micron and submicron-sized materials composed of one-pot mixture of iron oxysulfide and iron oxide. The final compound as well as reference materials greigite and magnetite were investigated by powder X-ray diffraction (XRD), scanning electron microscopy (SEM), and energy dispersive X-ray (EDX) spectroscopy. The crystal structure, chemical composition, and morphology of the particles of the iron oxysulfide/iron oxide composite were compared to the ones of the references, iron sulfide and iron oxide. The materials showed clear differences both in reduction and oxidation when they were cycled between 0.1-3.0 V or 1.0-3.0 V vs. Li⁺/Li. In all cases, electrochemical properties of the iron oxysulfide/iron oxide mixture make out to the ones of two reference materials. The in situ XRD investigation of greigite nanoplatelets confirmed that a topotactic reaction occurs between 3.0 and 1.0 V vs. Li⁺/Li, followed by a conversion reaction at potentials negative to 1.0 V vs. Li⁺/Li during the first lithiation.

1. Introduction

Over the last two decades, the increased demand for portable energy storage has driven research and development activities towards the development of more efficient and less expensive lithium-ion batteries (LIBs). To increase the specific energy and power density of today LIBs, novel electroactive materials need to be designed.

Spinel (space group *Fd-3m*) constitute a large class of transition metal inorganic compounds adopting the generic formula of (A_{1-x}B_x)[A_xB_{2-x}]X₄, where heterovalent A and B cations are distributed in a tetrahedral and two octahedral sites (in parenthesis and square brackets, respectively) following an inversion rate *x*, in a cubic close-packed array of divalent anions (X= O, S, Se or Te).^{1, 2} Various spinels can be designed via ionic substitution, but nonstoichiometric spinels also exist. Cationic overstoichiometry and accommodation of vacancies in the anionic network are two approaches which have been already used to design promising electroactive materials.^{3, 4}

The electrochemical properties of magnetite Fe₃O₄ were first investigated by Thackeray et al. in the early 1980s.⁵ Lithium insertion (reduction) was described as the successive formation of Li_xFe₃O₄ intermediates until the reversible

formation of Li₂O and extrusion of metallic iron.⁵ Later, this conversion reaction mechanism, $M_nX_z + 2z e^- + 2z Li^+ = z/2 Li_2X + x M^0$ (with X = O, S...), was elucidated by Poizot et al.⁶ However, the high volume changes that occur during the conversion reaction are a challenge for the long-term electrochemical stability of the electrodes.⁶⁻⁸ Improvements in the engineering of Fe₃O₄ electrodes have demonstrated the potential of spinel compounds: Ito et al. measured a reversible specific charge close to the theoretical value of 926 mAh/g,⁹ and later, Taberna et al. maintained 80% of the theoretical specific charge at a fast rate (less than 8 min) during 100 cycles.¹⁰ Other studies were reported in the literature combining Fe₃O₄ and graphene (to improve the conductivity of the material) and possess a reversible specific charge of 1200 mAh/g along 50 cycles.^{11, 12}

Greigite (Fe₃S₄) can be synthesized by diverse routes including solvothermal,¹³ coprecipitation,¹⁴ and single-source precursor¹⁵ methods. This metastable material, isostructural to magnetite,¹⁶ has been investigated as an electroactive material only one time.¹⁷ The specific charge reported of 110 mAh/g is encouraging, but it is still far below the theoretical value of 725 mAh/g and the reaction mechanism remained unknown.

Recently, Ludi et al.¹⁸ revealed a new approach to the synthesis of metal sulfides by an adaptation of the benzyl alcohol route.¹⁹⁻²¹ The low temperature route can be seen as an easy accessible method to synthesize nano- or submicron-sized particles of Fe₃X₄ (X= O, S) using mixtures of benzyl alcohol and benzyl mercaptan as solvent and co-reactants. To the best of our knowledge, the impact on chemical

^a Paul Scherrer Institute, Electrochemical Energy Storage Section, CH-5232 Villigen PSI, Switzerland.

† sebastien.sallard@psi.ch.

Electronic Supplementary Information (ESI) available: [details of any supplementary information available should be included here]. See DOI: 10.1039/x0xx00000x

substitution on the anionic site in transition metal spinels has not received any specific attention. However, this crystal-chemistry approach, primarily used to design positive electrodes for microbatteries, generally leads to metal oxysulfides with intergrowth of sulfide and oxide layers.^{22, 23} In the present work, we aimed to synthesize iron oxysulfide spinels by an easy and up scalable low temperature route. We compared their electrochemical properties with the one of the greigite and of the magnetite to investigate the influence of the anionic network of iron spinels. The materials were characterized using X-ray diffraction (XRD) combined with Rietveld refinement, as well as scanning electron microscopy (SEM). Their electrochemical properties were evaluated versus lithium in a half-cell configuration.

2. Experimental

2.1 Synthesis

In a 50 mL three-necked round-bottom flask, iron(III) acetylacetonate, $\text{Fe}(\text{C}_5\text{H}_7\text{O}_2)_3$ (2 mmol, 97%, Aldrich) was combined with benzyl alcohol (benzyl-OH, 99%, Alfa Aesar) and benzyl mercaptan (benzyl-SH, 99%, Alfa Aesar) as both solvent and reactant. The molar ratio of the iron precursor and solvent was 1/50. Mixed benzyl-SH/benzyl-OH solutions were defined as: x benzSH + $(1 - x)$ benzOH, with x being the mixing parameter in terms of molar ratio. After the mixture was stirred and sparged with Ar for 30 min, it was heated at 175°C for 40 h under Ar atmosphere. Then, the mixture was cooled to room temperature, extracted with acetone (Alfa Aesar), centrifuged, and washed two times with acetone. Finally, the solid product was dried at 60°C and ground by hand. Three samples were prepared: reference materials greigite ($x = 1$) and magnetite ($x = 0$), and an oxysulfide material ($x = 0.25$).

2.2 Structural and morphological investigation

XRD patterns were recorded at room temperature over the 9.5–136.0° (2 θ) angular range with a 0.033° step and a scan speed of 0.16°/min, using a PANalytical Empyrean diffractometer equipped with a Cu-anti cathode ($\lambda = 1.54060$, 1.54442 Å). Rietveld refinements were performed using the program FullProf.²⁴ Experimental diffraction patterns were fitted using a Finger-Cox-Jephcoat pseudo-Voigt function without any additional constraints. The profile analysis is based on the angular dependence of the full-width-at-half-maximum (FWHM) of the Gaussian (H_G) and Lorentzian (H_L) components, where the instrumental and the sample intrinsic contributions (microstructural analysis, see Supplementary Information) to the diffraction peak broadening are examined separately.^{25, 26} The resolution function of the diffractometer was extracted from the diffraction pattern of the standard powder LaB_6 .^{27, 28} The SEM images were recorded for each powder sample using a Carl Zeiss UltraTM 55 (Germany) apparatus at 3 kV tension using the in-lens detector. Energy dispersive X-ray spectroscopy (EDX) measurements were also performed.

2.3 Cell preparation and electrochemical measurements

The active materials (greigite, magnetite, or iron oxysulfide/iron oxide composite) were mixed with Super C carbon black (Imerys Carbon and Graphite, Switzerland) and Kynar FLEX 2801 PVDF binder in a weight ratio of 80/10/10, respectively, and dispersed in *N*-methylpyrrolidone. The slurry was cast onto copper foil. After drying at 120°C under vacuum overnight, the electrodes were punched and directly introduced in an Ar-filled glove box. Half-cells were assembled with LP30 (1 M LiPF_6 in 1:1 (w/w) ethyl carbonate:dimethyl carbonate) as electrolyte, Li metal as the counter electrode, and glass fibers as the separator. The cells were electrochemically cycled in two potential ranges, 1.0 and 3.0 V and 0.1 and 3.0 V vs. Li^+/Li , by cyclic voltammetry (scan rate: 50 $\mu\text{V/s}$) and galvanostatic cycling ($j_m = 34$ mA/g, see Supplementary Information). All potentials are given compared to the Li^+/Li reference. A free-standing film with the same 80/10/10 composition was assembled in a homemade XRD cell for *operando* XRD analysis.²⁹

3. Results and discussion

3.1 Structural characterization

The active material powders were synthesized in pure benzyl-OH, pure benzyl-SH, and a mixture of the two with $x = 0.25$, and their X-ray diffraction patterns are presented in Figure 1. More details of the microstructure analysis are presented in the Supplementary Information.

The diffraction pattern of the one-pot composite ($x = 0.25$) presented in Figure 1a reveals a biphasic nature of the powder. The XRD pattern was indexed with two cubic cells ($Fd\bar{3}m$ space group $n^\circ 227$) having unit cell parameters of 9.850(1) and 8.389(1) Å. Rietveld refinements suggested the presence of 75% of an iron sulfide spinel and 25% of an iron oxide. The diffraction peaks of the iron sulfide are reasonably narrow (FWHM of 0.66 for the (311) reflection), and the $hk0:h = k = 2n$ reflections are asymmetric on the left side of their respective peaks, suggesting structural distortions or chemical inhomogeneities. Rietveld refinements indicated that the iron sulfide consisted of a greigite-like compound with the presence of iron(II) vacancies in the B sites, leading to a chemical composition type of $(\text{Fe}^{3+}_1)[\text{Fe}^{3+}_{1.08}\text{Fe}^{2+}_{0.88}]\text{S}_4$, when the occupation rate of S is constrained. Releasing this later parameter leads to divergence of profile parameters, high isotropic displacement parameter ($B_{iso} = 1.55(1)$ Å²) and non-physical value of the occupation rate itself. The partial substitution of sulfur for oxygen anions maintains the refinement stable and lowers the B_{iso} value to 0.676(1) Å², for a chemical composition of $\text{Fe}_{2.96}\text{S}_{3.72}\text{O}_{0.28}$. The Rietveld refinement also showed that the iron oxide accompanying the iron oxysulfide consisted of a highly crystallized $\gamma\text{-Fe}_2\text{O}_3$ maghemite (sharp Lorentzian diffraction peaks with a FWHM of the (311) reflection = 0.23).

This results show that the formation of an oxysulfide occurred during the one-pot composite preparation, nevertheless the

distribution of oxygen in the anionic network of the greigite cannot be discussed by powder x-ray diffraction analyses.

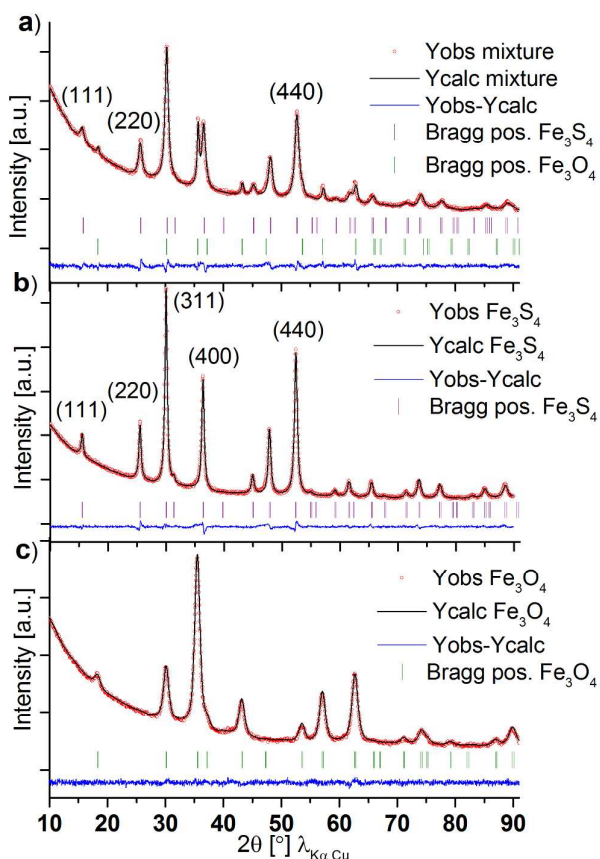


Figure 1: XRD Rietveld refinements (red dots: experimental data; black continuous lines: calculated curve; blue continuous lines: difference between the calculated and experimental data; purple bars: Bragg contributions of greigite; green bars: Bragg contributions of magnetite) of the materials synthesized in a) $x = 0.25$, b) Benzyl-SH ($x = 1$), and c) Benzyl-OH ($x = 0$).

The x-ray diffraction pattern of the product prepared by the benzyl-SH ($x = 1$) presented in Figure 1b is indexed in a cubic cell with unit cell parameter of $a = 9.845(1) \text{ \AA}$ ($Fd-3m$ space group). The diffraction peaks are quite sharp (FWHM of 0.47 for (311)) and adopt a Lorentzian profile shape ($\eta = 0.88$). The $hk0:h = k = 2n$ reflections are asymmetric on the left side of their respective peak maxima, and the (400) peak maximum is slightly shifted towards a smaller 2θ angle, suggesting the presence of intrinsic stacking faults.³⁰ The Rietveld refinement confirms the formation of pure greigite with benzyl-SH and converges to satisfying agreement factors ($R_B \approx 6$, $\chi^2 \approx 2.9$) with an inversion rate of 0.44, corresponding to a chemical composition of $(\text{Fe}^{3+}_{0.56}\text{Fe}^{2+}_{0.44})[\text{Fe}^{3+}_{0.56}\text{Fe}^{2+}_{1.44}]_4\text{S}_4$.

The x-ray diffraction pattern of the other reference material obtained in pure benzyl-OH (Figure 1c) was indexed in a cubic cell with $a = 8.381(1) \text{ \AA}$ ($Fd-3m$ space group). The diffraction peaks were broader and less Lorentzian than the greigite reflections (FWHM of the (311) reflection = 0.98; $\eta = 0.65$). The Rietveld refinement confirmed the formation of a single-

phased magnetite, and converged to satisfying agreement factors ($R_B \approx 5$, $\chi^2 \approx 1.15$) when iron(II) vacancies—labelled \square —were introduced in the B sites as follows: $\text{Fe}^{III}[\text{Fe}^{III}_{1+(2x/3)}\text{Fe}^{II}_{(1-x)}\square_{1/3}]_B\text{O}_4$. This can evoke a “surface oxidation” of the magnetite particles that shifts the chemical composition of the magnetite towards $(\text{Fe}^{3+})[\text{Fe}^{3+}_{5/3}\square_{1/3}]_B\text{O}_4$ known as maghemite $\approx \gamma\text{-Fe}_2\text{O}_3$.³¹

3.2 Morphological characterization

SEM micrographs of the as-synthesized samples and prepared electrodes are shown in Figure S1 and 2 respectively

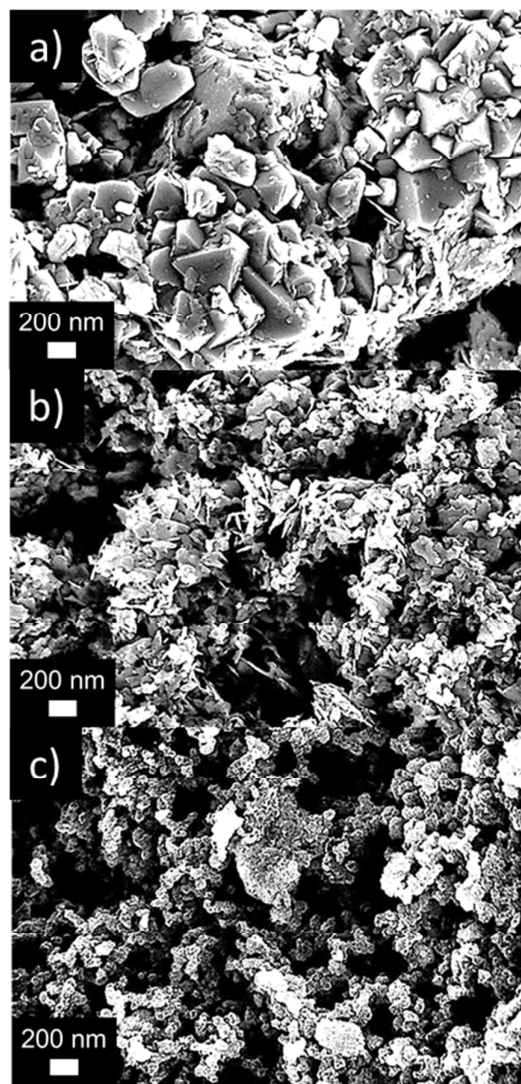


Figure 2: SEM micrographs of electrodes prepared with a) the oxysulfide/oxide composite ($x = 0.25$), b) greigite ($x = 1$), and c) magnetite ($x = 0$).

The micrograph of iron oxysulfide/oxide mixture presented in Figure 2a shows interlocked submicron- and micron-sized octahedral-shaped crystallites presenting smooth edges. The presence of micron-sized crystallites is consistent with the presence of narrow diffraction peaks in Figure 1a notably assigned to maghemite.

The micrograph in Figure 2b shows rounded agglomerates of greigite platelets, as observed by Paoletta et al.¹⁷ with an average length of 150 ± 50 nm and an average thickness of 15 ± 5 nm. The observed dimensions of these platelets are much larger than the average crystallite size L of 8.5 ± 0.5 nm estimated from the XRD microstructural analysis (Figure 1b). This confirms the presence of structural or microstructural defects in the greigite particles highlighted by the high degree of microstrain calculated during microstructural analyses ($\epsilon \approx 3.3 \times 10^{-3}$, see Supplementary Information).

The micrograph in Figure 2c reveals coarse spherical agglomerates with a size distribution between 20 and 250 nm and lower roughness compared to the greigite particles (Figure 2b). The spherical primary particles of magnetite have a diameter of 20 ± 5 nm (Figure S2) which is in good agreement with the average crystallite size estimated from the microstructural analysis ($L = 8.5 \pm 0.5$ nm, $\epsilon \approx 5.8 \times 10^{-3}$, see Supplementary Information). Similar morphologies and particles sizes for Fe_3O_4 nanoparticles synthesized in benzyl-OH were reported in the literature.^{11, 12, 21}

Thus, structural and morphological characterizations of the Fe_3X_4 ($X = \text{O}, \text{S}$) materials synthesized via low temperature route have showed that, in the case of $x = 0.25$, the iron sulfide $\text{Fe}_{2.96}\text{S}_{3.72}\text{O}_{0.28}$ and the iron oxide $\gamma\text{-Fe}_2\text{O}_3$ clearly differ in terms of chemical composition and microstructure from the materials synthesized with $x = 0$ and 1. In the rest of the manuscript, the prepared materials will be referred to as iron oxysulfide/oxide composite (IOOC) for $x = 0.25$, greigite for $x = 1$, and magnetite for $x = 0$.

3.3 Electrochemical characterization

3.3.1 Specific charge

The evolution of the specific charge vs. cycle number for the three materials cycled between 1.0 and 3.0 V is shown in Figure 3a. For the IOOC sample, the initial specific charge of 620 mAh/g fades dramatically to reach only 32 mAh/g after 20 cycles. The greigite shows a high specific charge of 1000 mAh/g in the first discharge; nevertheless, the specific charge is only 30 mAh/g after 20 cycles. The IOOC material shows however after the eighth cycle a better specific charge retention compared to the greigite. The magnetite has a lower initial specific charge of only 255 mAh/g during discharge, and reaches only 55–60 mAh/g after 20 cycles.

When focusing on the cycling performance in the 0.1–3.0 V potential window (Figure 3b), the three materials show non-negligible differences compared to the 1.0–3.0 V potential

window. The IOOC material shows an initial specific charge of 1300 mAh/g and then rapidly fades, reaching a value of 15–20 mAh/g in the 12th cycle; thereafter, it remains quasi-constant. The greigite has an initial specific charge of 1875 mAh/g in discharge, however, it also rapidly fades to reach 90 mAh/g in the 12th cycle, where it then remains stable. The magnetite has an initial specific charge of 1800 mAh/g. Thereafter, it decreases rather rapidly, but at a slower rate than the specific charge of greigite, to reach a value 215 mAh/g in the 20th cycle.

The total specific charge of each material is much higher than the theoretical value. In the first reduction, the formation of a passivation layer is certainly an important contributor to this extra specific charge but it cannot be the only one. This phenomenon can be rather attributed to the nanosize effect,^{32–34} with possible storage of charge at the surface.³⁵ The lower stability of the IOOC in the 0.1–3.0 V potential window as compared to the other materials can be attributed to a morphological effect as indicated in the SEM results as well as a possible volume change during cycling. The contact loss in the electrode due to volume changes during cycling will then be more dramatic for materials with micrometer-size particles ($x = 0.25$) than nanometer ones ($x = 1$ and 0).

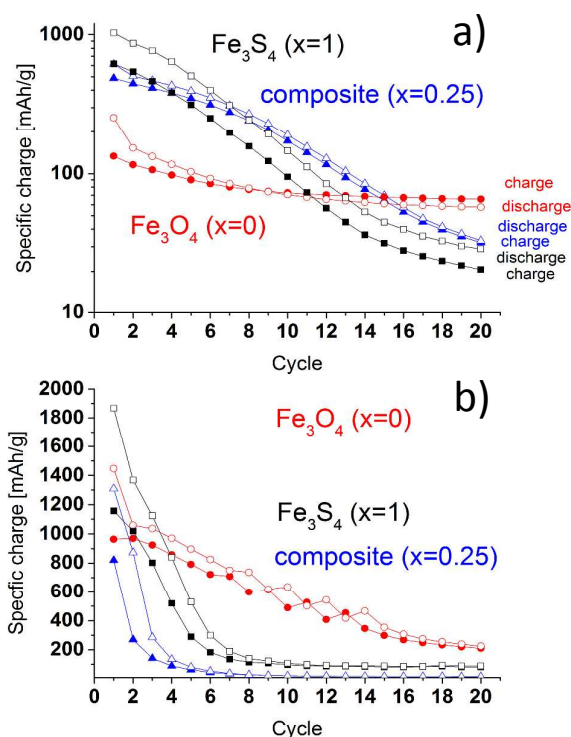


Figure 3: Evolution of the specific charge for the IOOC (triangle), greigite (square), and magnetite (circle) cycled between a) 1.0 and 3.0 V and b) 0.1 and 3.0 V.

The normalized galvanostatic curves of IOOC and greigite materials (Figure S3) show a continuous increase of the overpotential during the first five cycles. This overpotential is

even more pronounced for the 0.1–3.0 V potential window than for the 1.0–3.0 V one. We attribute this overpotential built-up to an increase of the resistance. By opposition, the galvanostatic curves of the magnetite electrodes present a quasi-monotonous hysteresis in agreement with a stable specific charge in the first cycles (Figure 3).

We assume that the IOOC and greigite materials suffer from low conductivity and high overpotential, mainly due to an insulation of the particles during cycling (thick SEI). To confirm the influence of the low conductivity, we tested electrodes composed of the active materials mixed in equivalent ratio (1:1) with conductive carbon SuperC65. As expected, the greigite and composite materials (Figure S4) present a significant improvement of the specific charge during cycling.

3.3.2 Cyclic voltammetry of the IOOC ($x = 0.25$)

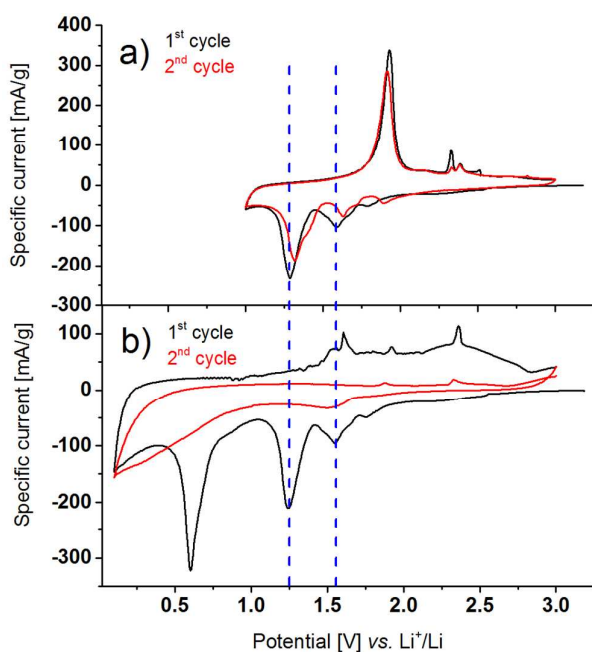


Figure 4: Cyclic voltammograms in the a) 1.0–3.0 V and b) 0.1–3.0 V potential windows for the IOOC.

The IOOC was cycled using two protocols: i) between 1.0 and 3 V and ii) between 0.1 and 3 V. In the 1.0–3.0 V potential window, the first cycle (Figure 4a) shows two cathodic peaks at 1.29 and 1.59 V, with the first having greater magnitude. During the first oxidation (Figure 4a), two anodic peaks at 1.93 and 2.3 V may be observed, however, the second peak has a minor contribution. In subsequent cycles, the behavior is the same. In this potential window the reaction is reversible. This could be a hint that the reaction mechanism is based on the (normally reversible) insertion rather than on the (normally irreversible) conversion.

Table 1. Principal CV peaks for the prepared materials in the 1.0–3.0 and 0.1–3.0 V potential windows.

Potential window	IOOC		Greigite		Magnetite	
	Reduction	Oxidation	Reduction	Oxidation	Reduction	Oxidation
1 st cycle potential [V] vs. Li ⁺ /Li ⁺						
1–3.0 V	1.79	1.93	1.61	1.90	1.50	2.43
	1.59	2.33	1.37	2.40		
	1.29	2.40				
	1.79	1.54	1.61	1.47	1.50	1.68
0.1–3.0 V	1.59	1.60	1.37	1.90	0.93	1.82
	0.6	1.92	0.77	2.40	0.62	
		2.36				

*The most intense peaks are indicated in bold. Values in red indicate behavior similar to that observed in the IOOC sample.

When reduced below 1.0 V (Figure 4b), the first cycle shows an additional cathodic peak at 0.6 V preceded by a broadening at 0.85 V. The broadening at 0.85 V could be attributed to solid electrolyte interphase (SEI) formation. The first oxidation shows no significant oxidation peak and only 2 broad peaks located at 1.5 and 2.5 V. All cathodic peaks are smeared in the subsequent cycle; only a broad, weak cathodic peak is visible at 1.5 V as well as two weak anodic peaks at 1.9 and 2.35 V. The principal peak potentials in the first cycle between the 1.0–3.0 V and 0.1–3.0 V potential windows are summarized in Table 1.

For the sake of clarity, we compared the IOOC results to those for greigite and magnetite.

3.3.3 Cyclic voltammetry of greigite ($x = 1$)

In the potential window between 1.0 and 3 V (Figure 5a), the first cycle for greigite shows two cathodic peaks, a main one at 1.61 V and a minor one at 1.37 V. In the oxidation step, two peaks are observed at 1.90 and 2.40 V. The position and the profile of the redox peaks are similar in the subsequent cycle. During the first reduction at a potential lower than 1.0 V (Figure 5b), a third cathodic peak is present at 0.77 V. A new broad anodic peak appears at 1.46 V, followed by two peaks at 1.9 and 2.4 V. All the peaks are smeared out in the subsequent cycle; two cathodic peaks are present at 0.72 and 1.54 V, and one anodic peak occurs at 1.47 V as well as a doublet at 2.30 and 2.42 V.

The cathodic peak at around 0.77 V (Figure 5b) can be attributed to the formation of the SEI,³⁶ via the irreversible degradation of organic compounds in the electrolyte and/or the reaction of the greigite.

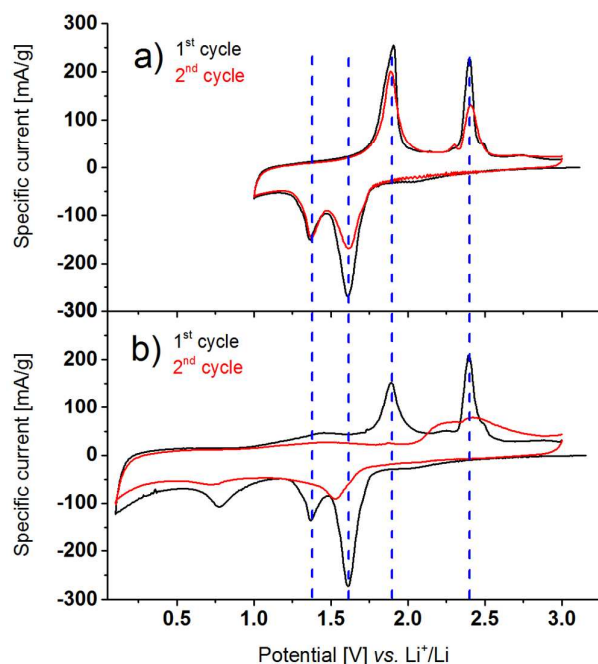


Figure 5: Cyclic voltammograms for greigite ($x = 1$) in the a) 1.0–3.0 V and b) 0.1–3.0 V potential windows.

3.3.4 Cyclic voltammetry of magnetite ($x = 0$)

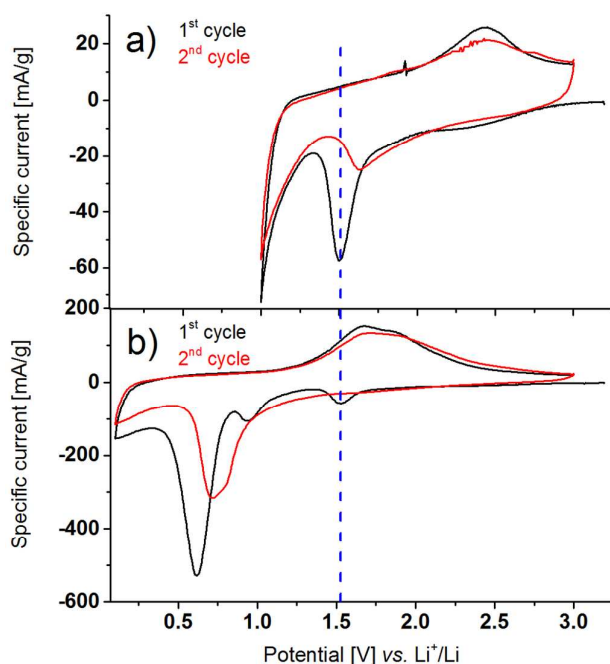


Figure 6: Cyclic voltammograms for magnetite ($x = 0$) in the a) 1.0–3.0 V and b) 0.1–3.0 V potential windows.

In the potential window between 1.0 and 3.0 V, magnetite presents a sharp cathodic peak at 1.5 V (Figure 6a). The

cathodic peak dramatically disappears and is replaced by one at 1.63 V in the subsequent cycle. The broad anodic peak at 2.43 V is a signature for the extraction of Li^+ from lithiated iron oxides.³⁵

When magnetite is cycled in the 0.1–3.0 V range (Figure 6b), another small cathodic peak is visible at 0.95 V, followed by a significant peak at 0.62 V. The main cathodic peak in the subsequent cycle is less intense and shifted from 0.7 to 0.8 V.^{12, 37} Two broad anodic peaks, visible at 1.65 and 1.85 V, are attributed to the oxidation of Fe^0 into Fe^{2+} and then Fe^{3+} , respectively.³⁸

3.3.5 Electrochemical results-Discussion

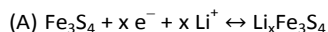
A close comparison of CVs of the IOOC with the two reference samples, greigite and magnetite, reveals that the electrochemical properties, of the IOOC differs to the combination of the electrochemical properties of the two reference properties, as a hybrid material. This observation is in concordance with the conclusions from the structural and morphological characterizations, part 3.1 and 3.2 respectively. In the 1.0–3.0 V potential window, we observe that, during lithiation, the main phenomenon occurring at 1.29 V is at a potential below that observed in greigite (1.37 V) and far from that of magnetite (1.5 V). This difference can be explained by the partial substitution of S for O and the amount of chemical/structural defects in the material as suggested by the Rietveld refinements. On delithiation, the reaction pathways are similar for greigite and the IOOC, with the main phenomenon occurring at 1.9 V. If we carefully consider the corresponding magnetite reaction that occurs at 2.43 V, we see that the potentials are similar for the IOOC and the magnetite, indicating no modification of the spinel structure. These results indicate that the overpotential is more important in the case of the IOOC than the greigite material and the magnetite has no one. The overpotential observed for the one pot composite can be explained by the large size and the anisotropic behavior of the particles, limiting the rate of the in and out lithium diffusion through the bulk.

The same conclusion can be drawn from the experiments in the larger potential window (0.1–3 V) where we see that the overpotential is again larger when comparing the greigite and the IOOC, whereas no overpotential can be observed between the IOOC and the magnetite.

In summary, we have demonstrated that preparation of an oxysulfide is feasible, even if it is mixed with a metal oxide phase. Additionally, the IOOC cycles differently than reference materials, greigite and magnetite.

Moreover, we wanted to better understand the reaction mechanism for greigite during cycling, and after careful analysis, we suggest the following hypothesis: An insertion reaction (A) occurs during cycling in the 1.0–3.0 V potential window due to the highly reversible behavior between the first and second cycles. For the potential window between 0.1–3.0 V, the process changes and the material tends to undergo the conversion reaction (B), as can be seen from the different

electrochemical behavior during the first and the second cycles.



It may appear inconsistent to claim that the greigite reacts in the potentials below 1 V via a conversion reaction (B), when same oxidation peaks at 2.30 and 2.42 V are observed for the first cycle in the Figure 1.a [reaction (A) only] and Figure 1b [reactions (A) and (B)]. First, we notice that the relative intensities for the anodic peak doublet are inverted between the Figure 1a and the Figure 1b. It suggests that the oxidation processes are not exactly the same after a reduction until 1 V (Figure 1a) and until 0.1 V (Figure 1b). In the second point, a partial reformation of greigite during the first oxidation can occur similarly to metal oxide materials.^{6, 39}

3.3.6 In situ XRD study of greigite

To confirm our assumption of a conversion reaction, we performed an in situ XRD study with greigite (Figure 7). The X-ray diffraction pattern do not show any significant change until reaching 1.75 V. Longer reduction shifts the maxima of the diffraction peaks of greigite to lower angles, and we observe broadening of the diffraction peaks and decrease in their intensities (blue line at 1.33 V). The diffraction peaks of greigite completely disappear at 1 V.

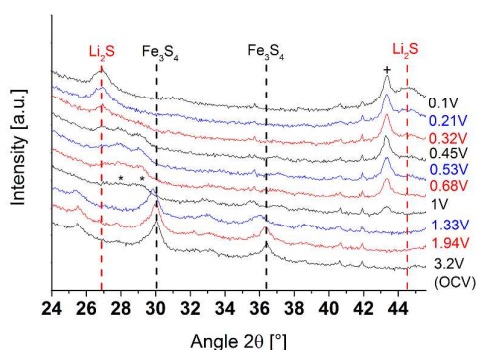


Figure 7: In situ XRD patterns collected during the first reduction step of the greigite. Cross (+) and star (*) symbols are ascribed to a probable new phase(s) “ $\text{Li}_x\text{Fe}_y\text{S}_z$ ”.

We observe, at the same potential of 1 V, new unidentified peaks between 26.6–29.7° (marked by *) and at 43.3° (marked by +); they grow until the potential decrease to a value of ca. 0.45 V. Further reduction leads to the disappearance of the peaks between 26.6–29.7° at ca. 0.2 V while the peak at 43.3° stays constant. Simultaneously, for potential of ca 0.5 V, peaks at 26.9° and 44.6° appear and constantly grow until the end of the first reduction at 0.1 V. This first changes between OCV and 1.3 V are attributed to an insertion reaction with a low Li^+ level content in a spinel-type structure.⁴⁰ The unidentified peaks (*) and (+) between 1 V and ca. 0.4 V are ascribed to a

probable new phase(s) type “ $\text{Li}_x\text{Fe}_y\text{S}_z$ ” as has been described for $\text{Li}_x\text{Fe}_3\text{O}_4$ and $\text{Li}_x\text{Fe}_2\text{O}_3$.^{5, 41} The later peaks present at 26.9° and 44.6° between ca. 0.5 V and 0.1 V are attributed to the formation Li_2S . These data are in agreement with insertion (A) and conversion (B) mechanism from OCV to 1 V and from 1 V to 0.1 V, respectively (see part 3.3.5)

4. Conclusion

We presented an anhydrous one-pot synthesis that generated a composite material partially composed of oxysulfide. This demonstrated the possibility of the partial substitution of sulfur by oxygen using a soft chemistry route. Nevertheless, the synthesis led mainly to an oxysulfide/oxide composite with a microstructure that was close to but not identical with the synthesized pure greigite and magnetite materials.

The electrochemical properties of the oxysulfide/oxide composite were different than a simple mixture of the two iron sulfide and oxide materials. For potentials above 1.0 V, the oxysulfide/oxide composite had an initial specific charge higher than magnetite, with less capacity fading than greigite but a bigger overpotential. Optimization of the engineering of the electrode may increase the stability of the specific charge of this material.

Finally, the reaction mechanism for greigite under discharge conditions was investigated by in situ XRD, revealing a two-step process: (A) an insertion reaction between 1.0 and 3.0 V and (B) a conversion reaction leading to Li_2S formation at potentials below 1.0 V. This confirmed the high volume changes that occur during cycling and explained the poor cyclability of the material in the 0.1–3.0 V potential window.

Acknowledgements

Dr. Peter Bleith is warmly thanked for his help with the in situ measurement of the greigite. BASF SE is thanked for financial support. The authors are grateful to Dr. Cyril Marino for his help with SEM measurements.

Notes and references

- H. S. C. Oneill and A. Navrotsky, *Am. Miner.*, 1983, **68**, 181.
- S. H. Wei and S. B. Zhang, *Phys. Rev. B*, 2001, **63**, 8.
- J. M. Tarascon, W. R. McKinnon, F. Coowar, T. N. Bowmer, G. Amatucci and D. Guyomard, *J. Electrochem. Soc.*, 1994, **141**, 1421.
- B. Scrosati, *Electrochim. Acta*, 2000, **45**, 2461.
- M. M. Thackeray, W. I. F. David and J. B. Goodenough, *Mater. Res. Bull.*, 1982, **17**, 785.
- P. Poizot, S. Laruelle, S. Grugeon, L. Dupont and J. M. Tarascon, *Nature*, 2000, **407**, 496.
- P. Poizot, S. Laruelle, S. Grugeon, L. Dupont and J. M. Tarascon, *J. Power Sources*, 2001, **97-98**, 235.
- A. Débart, L. Dupont, P. Poizot, J.-B. Leriche and J. M. Tarascon *J. Electrochem. Soc.*, 2001, **148**, A1266.

9. S. Ito, K. Nakaoka, M. Kawamura, K. Ui, K. Fujimoto and N. Koura, *J. Power Sources*, 2005, **146**, 319.
10. L. Taberna, S. Mitra, P. Poizot, P. Simon and J. M. Tarascon, *Nature Mater.*, 2006, **5**, 567.
11. S. Baek, S.-H. Yu, S.-K. Park, A. Pucci, C. Marichy, D.-C. Lee, Y.-E. Sung, Y. Piao and N. Pinna, *RSC Adv.*, 2011, **1**, 1687.
12. S. H. Yu, D. E. Conte, S. Baek, D. C. Lee, S. K. Park, K. J. Lee, Y. Piao, Y. E. Sung and N. Pinna, *Adv. Func. Mater.*, 2013, **23**, 4293.
13. Z. J. Zhang and X. Y. Chen, *J. Alloy. Comp.*, 2009, **488**, 339.
14. Y.-S. Chang, S. Savitha, S. Sadhasivam, C.-K. Hsu and F.-H. Lin, *J. Colloid Interf. Sci.*, 2011, **363**, 314.
15. J. H. L. Beal, P. G. Etchegoin and R. D. Tilley, *J. Phys. Chem. C*, 2010, **114**, 3817.
16. B. J. Skinner, F. S. Grimaldi and R. C. Erd, *Am. Miner.*, 1964, **49**, 543.
17. A. Paoletta, C. George, M. Povia, Y. Zhang, R. Krahne, M. Gich, A. Genovese, A. Falqui, M. Longobardi, P. Guardia, T. Pellegrino and L. Manna, *Chem. Mat.*, 2011, **23**, 3762.
18. B. Ludi, I. Olliges-Stadler, M. D. Rossell and M. Niederberger, *Chem. Commun.*, 2011, 5280.
19. I. Bilecka, I. Djerdj and M. Niederberger, *Chem. Commun.*, 2008, 886.
20. N. Pinna and M. Niederberger, *Angew. Chem. Inter.*, 2008, **47**, 5292.
21. N. Pinna, S. Grancharov, P. Beato, P. Bonville, M. Antonietti and M. Niederberger, *Chem. Mat.*, 2005, **17**, 3044.
22. S. Indris, J. Cabana, O. J. Rutt, S. J. Clarke and C. P. Grey, *J. Am. Chem. Soc.*, 2006, **128**, 13354.
23. S. K. Singh, A. Kumar, B. Gahtori, Shruti, G. Sharma, S. Patnaik and V. P. S. Awana, *J. Am. Chem. Soc.*, 2012, **134**, 16504.
24. J. Rodrigue-Carvajal, *Physica B*, 1993, **192**, 55.
25. A. Leineweber, *Z. Kristallogr.*, 2011, **226**, 905.
26. J. Rodriguez-Carvajal and T. Roisnel, in *European Powder Diffraction Epdic 8*, eds. Y. Andersson, E. J. Mittemeijer and U. Welzel, 2004, vol. 443-4, pp. 123-126.
27. P. Karen and P. M. Woodward, *J. Solid State Chem.*, 1998, **141**, 78.
28. D. Balzar, N. Audebrand, M. R. Daymond, A. Fitch, A. Hewat, J. I. Langford, A. Le Bail, D. Louer, O. Masson, C. N. McCowan, N. C. Popa, P. W. Stephens and B. H. Toby, *J. Appl. Crystallog.*, 2004, **37**, 911.
29. P. Bleith, H. Kaiser, P. Novák and C. Villevieille, *Electrochim. Acta*, 2015, in press, DOI: 10.1016/j.electacta.2015.06.105.
30. A. I. Ustinov and N. M. Budarina, *Powder Diffr.*, 2002, **17**, 270-277.
31. S. H. Sun and H. Zeng, *J. Am. Chem. Soc.*, 2002, **124**, 8204-8205.
32. J. M. Yan, H. Z. Huang, J. Zhang, Z. J. Liu and Y. Yang, *J. Power Sources*, 2005, **146**, 264.
33. C. Wu, Q. C. Zhuang, Y. X. Wu, L. L. Tian, X. X. Zhang and S. G. Sun, *Func. Mat. Lett.*, 2013, **6**.
34. D. Larcher, D. Bonnin, R. Cortes, I. Rivals, L. Personnaz and J. M. Tarascon, *J. Electrochem. Soc.*, 2003, **150**, A1643.
35. S. Komaba, T. Mikumo, N. Yabuuchi, A. Ogata, H. Yoshida and Y. Yamada, *J. Electrochem. Soc.*, 2010, **157**, A60.
36. S. Laruelle, S. Grugeon, P. Poizot, M. Dolle, L. Dupont and J. M. Tarascon, *J. Electrochem. Soc.*, 2002, **149**, A627.
37. Y. He, L. Huang, J.-S. Cai, X.-M. Zheng and S.-G. Sun, *Electrochim. Acta*, 2010, **55**, 1140.
38. J. Morales, L. Sánchez, F. Martín, F. Berry and X. Ren, *J. Electrochem. Soc.*, 2005, **152**, A1748.
39. P. Poizot, S. Laruelle, S. Grugeon and J. M. Tarascon, *J. Electrochem. Soc.*, 2002, **149**, A1212.
40. J. Rodríguez and J. Fontcuberta, *J. Mater. Sci*, 1987, **22**, 1001.
41. M. Pernet, P. Strobel, B. Bonnet, P. Bordet and Y. Chabre, *Solid State Ionics*, 1993, **66**, 259.

One-pot mixtures of magnetite Fe_3O_4 and greigite Fe_3S_4 powders were synthesized by sol-gel chemistry. Operando XRD measurements prove the conversion mechanism of the greigite reduction below 1.0 V vs. Li^+/Li .

